CHAPTER - 2

MATERIALS AND METHODOLOGY

2.1 SATELLITE DATA AND ITS CHARACTERISTICS

The multi-orbiting space platform with multi-spectral (optical) and microwave (SAR) satellite imagery data were used in this research work. The Sentinel - 1 A (C - band) and ALOS - 2 (L - band) SAR satellite data were used in the study, which is provided by European Space Agency (ESA) and Japan Aerospace Exploration Agency (JAXA), respectively. Also, the optical satellite images from Sentinel - 2, Landsat - 8, MODIS and PROBA - V were used in this research work.

2.1.1 Optical satellite data

Optical satellite data acquires images in the visible and infrared regions of the electromagnetic spectrum. Optical images can be displayed in natural colour (as visible to the human eye) and in false colour (with visible as well as infrared information). False colour images are useful for agricultural (crop classification), environmental (vegetation health) and geological applications (soil mapping). The optical satellite products were influenced by the atmospheric constituents, cloud and rain which hampered the image quality for precise study of Earth features. Therefore, the various atmospheric correction algorithms (ATCOR, FLAASH, ACORN, QUAC and MODTRAN) were used to enhance the optical image quality for better interpretation of Earth targets. In the present thesis work, the less contaminated and cloudy free date of acquisition of satellite images were considered for the study of spectral reflectance responses and derivation of spectral indices over the vegetation and soil surfaces.

2.1.1.1 Landsat – 8 (OLI) satellite data

Landsat-8 (OLI) data was launched in February 2013 by joint collaboration between NASA and the United States Geological Survey (USGS) and continues to acquire land surface data from space. It has a radiometric resolution of 12 - bits and temporal resolution of 16 days. There are 11 bands whose specification is provided in Table 2.1. The Landsat-8 Level - 3 product provides atmospheric, radiometric and geometric (terrain) corrected data. The quality of Landsat-8 Level-3 data is comparatively less contaminated by cloud and haze due to removal through cloud masking algorithm and precise calibration than Level - 2 and Level -1 product.

Table 2.1 The details specification of Landsat - 8 (OLI) satellite data

Bands	Wavelength range (µm)	Spatial resolution (m)
Band 1	0.43 – 0.45 (Aerosol)	30
Band 2	0.45 – 0.51 (Blue)	30
Band 3	0.53 – 0.59 (Green)	30
Band 4	0.63 – 0.67 (Red)	30
Band 5	0.85 – 0.88 (NIR)	30
Band 6	1.56 –1.65 (SWIR-1)	30
Band 7	2.10 - 2.29 (SWIR-2)	30
Band 8	0.50 – 0.67 (Panchromatic)	15
Band 9	1.36 –1.38 (Cirrus)	30
Band 10	10.6 – 11.2 (TIR-1)	100
Band 11	11.5 – 12.5 (TIR-2)	100

2.1.1.2 Sentinel -2 (MSI) satellite data

Sentinel-2, first launched on 23 June 2015, is a European EO satellite. Sentinel-2 data carries a single payload, the Multi - Spectral Instrument (MSI), that contains 13 bands from 0.4 µm to 2.2 µm in spectral range. The image pre-processing of Sentinel -2 data was done in SNAP v 6.0.6 and distributed under the GNU GPL license-3.0. The reflectance images were processed from Top – Of - Atmosphere (TOA) Level 1C S2, to Bottom – Of -Atmosphere (BOA) Level 2A using Sen2Cor processor. It has 10 days temporal resolution and 12-bit radiometric resolution. The details specification of bands is provided in Table 2.2.

Table 2.2 The spectral band specification of Sentinel - 2 (MSI) satellite data

Bands	Central wavelength (µm)	Spatial resolution (m)
Band 1	0.433 (Coastal aerosol)	60
Band 2	0.490 (Blue)	10
Band 3	0.560 (Green)	10
Band 4	0.665 (Red)	10
Band 5	0.705 (Red Edge)	20
Band 6	0.740 (Red Edge)	20
Band 7	0.783 (Red Edge)	20
Band 8	0.842 (NIR)	10
Band 8A	0.865 (Red Edge)	20
Band 9	0.945 (Water vapour)	60
Band 10	1.375 (SWIR -Cirrius)	60
Band 11	1.610 (SWIR)	20
Band 12	2.190 (SWIR)	20

2.1.1.3 Moderate Resolution Imaging Spectroradiometer (MODIS) global LAI data (MCD15A2H)

The global LAI data of MODIS is provided by the MCD15A2H Version-6 Level 4 products. This MODIS product provides 8-day composite dataset of the fraction of photosynthetically active radiation (FPAR) and leaf area index (LAI) images with 500-meter spatial resolution. The highly sensitive calibrated retrieval algorithm is used for providing the best pixel values from all the acquisitions of both MODIS sensors located on NASA's Terra and Aqua satellites from within the 8 - day period. The calibration of MODIS global LAI product may follow as:

$$\text{MODIS (LAI)} = \text{SF}^{\text{M}}.\ \text{DN} + \text{Offset} \qquad (2.1)$$

where DN is defined as digital number of image pixels and scaling factor (SF^{M}) value of MODIS is 1\10.

2.1.1.4 PROBA - V satellite data

The PROBA-V (Project for on-board Autonomy-Vegetation) satellite mission product provides the global LAI data at 300 m (version - 1) pixel size. The quality assessment of global LAI image was updated time to time for good precision and more agreement with ground level validation. The PROBA -V satellite data required to pixel calibration, which follows as:

$$\text{PROBA} - \text{V}\ \ (\text{LAI}) = \text{SF}^{\text{P}}.\ \text{DN} + \text{Offset} \qquad (2.2)$$

where DN is defined as digital number of image pixels and scaling factor (SF^{P}) value of PROBA -V is 1\30.

2.1.2 Synthetic aperture radar (SAR)

In the present thesis, the Sentinel - 1 A (C - band) and ALOS - 2 (L - band) SAR satellite images were used for biophysical and soil moisture retrieval using microwave scattering algorithms. The full details of SAR satellite data specification are shown in Table 2.3. Therefore, the details of pre-processing for SAR data and computation of backscattering coefficient (σ^0 (dB)) are discussed below in step by step.

Table 2.3 SAR satellite data characteristics

SAR characteristics	Sentinel -1A	ALOS -2
Launched date	3 April 2014	24 May 2014
Agency	ESA	JAXA
Frequency	C – band (5.405 GHz)	L – band (1.2 GHz)
Polarization	VV + VH	HH + HV
Spatial resolution	10 m	10 m
Temporal resolution	12 days	14 days
Incidence angle	25^0 - 43^0	8^0 - 70^0
Level of data	L 1	L 1.5

2.1.2.1 Sentinel – 1A SAR satellite data

Figure 2.1 shows the standard workflow to pre-process the Sentinel-1A SAR satellite data. The workflow was created in order to be used within the Sentinel application platform (SNAP) tool provided by European Space Agency (ESA). The processing graph in 'xml' format allows the processing of Sentinel-1A SAR data using the command line graph processing framework, which allows for batch processing of large datasets. The pre-processing workflow of SAR data consists of several major processing steps which reduces the error propagation in subsequent processes, described hereafter in separate subsections.

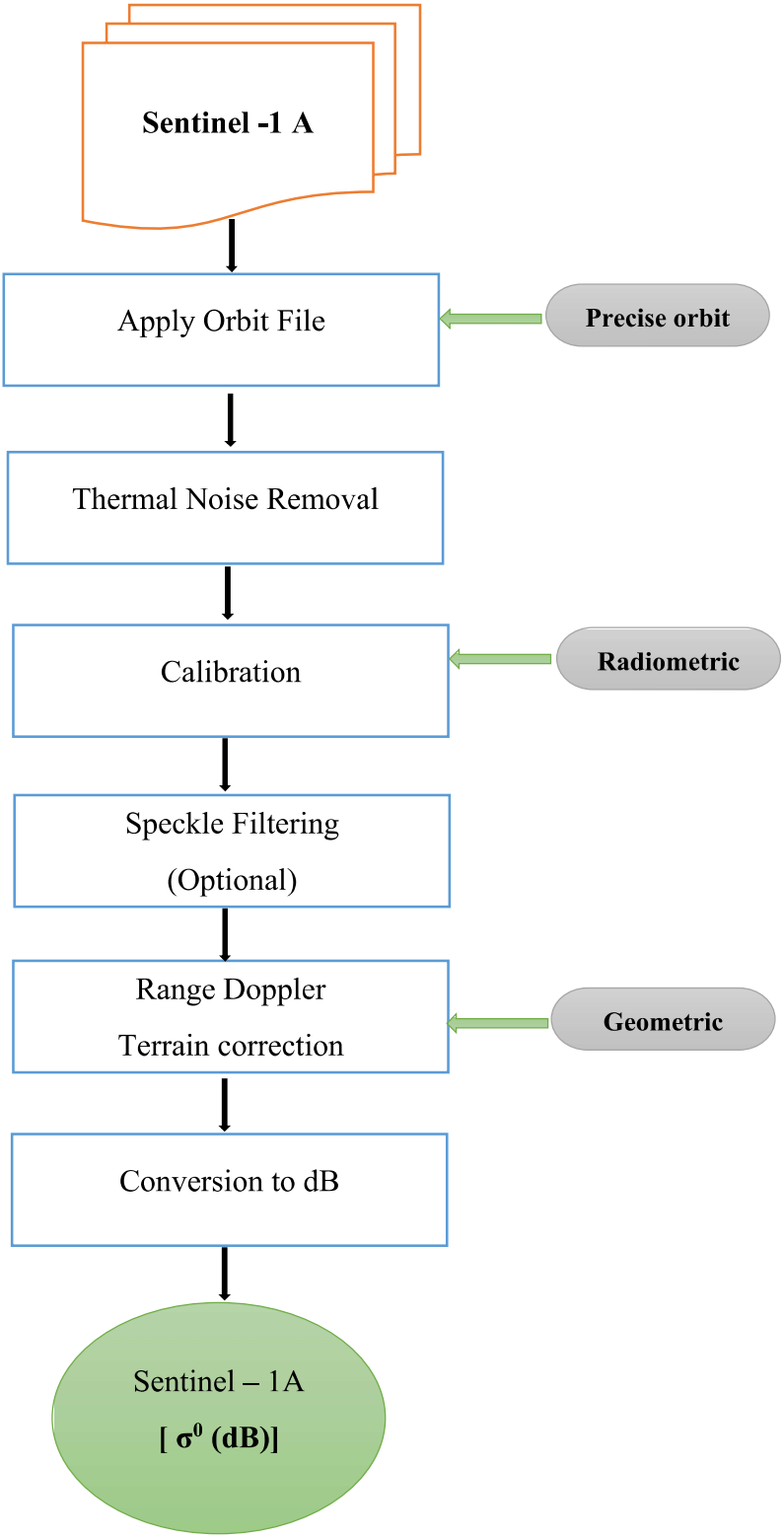

Figure 2.1 The detailed pre-processing workflow for Sentinel -1A synthetic aperture radar (SAR) satellite data

2.1.2.1.1 Apply Orbit File

The Sentinel-1A satellite orbit state vectors information was included within the metadata file of SAR products. The precise orbits of satellites are determined after several days and are available days-to-weeks after the generation of the product. The operation of applying a precise orbit available in SNAP allows the automatic download and update of the orbit state vectors for each SAR scene in its product metadata, providing an accurate satellite position and velocity information.

2.1.2.1.2 Thermal Noise Removal

Sentinel-1A satellite images are disturbed by additive thermal noise, particularly in the cross-polarization channel (VH polarization). Thermal noise removal reduces noise effects in the inter-sub-swath texture, in particular, normalizing the backscattering EMR signal within the entire Sentinel-1 image and resulting in reduced discontinuities between sub-swaths for scenes in multi-swath acquisition modes during satellite pass at define orbit. While generating level-1 products, the primary action is to correct the sampling start time in order to compensate for the change of the Earth's curvature. At the same time, azimuthal and range compression leads to radiometric effects at the image borders. The border noise removal algorithm, available as an operator in SNAP tool, was designed in order to remove low intensity noise and invalid data on scene edges during acquisition time.

2.1.2.1.3 Calibration (Radiometric correction)

The Sentinel -1A SAR satellite calibration is the procedure that converts satellite pixel values to radiometrically calibrated SAR backscattering coefficient. The information required to apply the calibration equation is included within the Sentinel - 1A GRD product; specifically, a calibration vector included as an annotation in the product allows simple

conversion of image intensity values into sigma nought (σ^0) values. In the designed pre - processing workflow, a LUT to produce σ^0 values is proposed, in order to generate radiometrically calibrated SAR backscattering EMR signal from Earth targets with respect to the nominally horizontal plane. The σ^0 has a significant variation with the incidence angle, wavelength, and polarisation, as well as with properties of the scattering surface (i.e. volume scattering, surface scattering and double bounce effect).

2.1.2.1.4 Speckle Filtering

The Speckle, appearing in Sentinel-1A SAR images as granular noise, is due to the interference of waves reflected from various scattering elements from the Earth surface. The Speckle filtering is a more important algorithm to increase SAR image quality by reducing speckle noises. The refined Lee filter was found to be more robust among all others speckle filters (Boxcar, Median, Frost, Gamma Map, Lee, Refined Lee, Lee Sigma and IDAN) available in the SNAP tool. The refined Lee filter having more visual interpretation, ability to preserve edges, linear features, and point target and texture information.

2.1.2.1.5 Range Doppler Terrain Correction (Geometric correction)

The Sentinel -1 A SAR data are generally sensed with a varying viewing angle greater than 0 degrees (30.74^0 – 46.25^0), resulting in images with some distortion related to side-looking geometry. Therefore, the geometric corrections are required to correct these distortions so that the geocoded satellite image will be as close as possible to the real world. The Range Doppler terrain correction is a correction caused by topography, such as foreshortening and shadows, using a digital elevation model (DEM) to correct the location (i.e. latitude and longitude) of each pixel. The target Coordinate Reference System (CRS) were chosen and optionally set to match the UTM zone (Zone – 44/45 and WGS 84). This

processing step allows the spatial setting of Sentinel-1A GRD products to Sentinel-2 MSI data grids, in order to develop the common spatial geolocation grid.

2.1.2.1.6 Conversion to dB

After all the major and necessary pre-processing steps of Sentinel-1A SAR data for the proper computation of the backscattering coefficient (m^2/m^2) is converted to decibel (dB) using a logarithmic transformation. Mathematically, the backscattering coefficient (σ^0 (dB)) can be computed using relation given as:

$$\sigma^0(dB) = 10 \times \log_{10} \frac{DN^2 \times \sin\theta}{A_{dn}^2 \times K} \qquad (2.3)$$

Where, DN is the Digital Number of the SAR satellite pixel value and A_σ is the SAR cross section. A_{dn} is the product final scaling from internal SLC to final GRD, K is the calibration constant and θ is the local incidence angle from the Earth targets to satellite altitude.

2.1.2.2 ALOS-2 SAR satellite data

The ALOS-2 SAR satellite images are Level - 1.5 products which have almost calibrated scene. However, some important correction is required like radiometric, terrain and speckle filtering. The single look complex (SLC) products were acquired for the study of present thesis work. Radiometric and terrain correction were performed using PolSARPro-v.6 tool, provided by ESA. Then after speckle filtering algorithm (Lee Sigma) was adopted for final calibration of this SAR images. The digital number (DN) were converted into SAR backscatter known as normalized radar cross section (NRCS). Thus, for the $\sigma^0(dB)$ of NRSC at the HH and HV polarization components can be obtained by the following formula with single calibration factor (CF), which can be expressed as follow:

$$\sigma^0(dB) = 10 \times \log_{10}(DN^2) - 83 \qquad (2.4)$$

2.2 COLLECTION OF GROUND TRUTH DATA

In this research work, the ground truth data were sampled in the years 2016 to 2019 during Rabi season (from December to March months) crop growth stages. During the field observations in the region of interest (ROI), various geolocations in the study regions were visited for the collection of in-situ measurements of biophysical and soil parameters on or near day of satellite image acquisition. These collected fields data will be helpful in the classification of vegetation and soil in the SAR satellite data. For the precise geolocation of the ground truth observations during field campaigns, the handheld global positioning system (GPS) receiver (Trimble Juno 3B) were used to capture the positional accuracy up to 5 meter in latitude and longitude coordinates.

2.2.1 Leaf area index (LAI) measurement

Leaf area index (LAI) is one of the key crop growth variables which decides the crop phenology and its health. Numerically, the LAI is defined as the ratio of one-sided leaf area to the unit area of the ground surface (i.e. unit of m^2/m^2). In the present thesis, an instrument LAI - 2200C Plant Canopy Analyzer (LI - COR, Inc.) was used for the measurement of LAI of the crops during acquisition of satellite overpasses in the sampling areas (Figure 2.1). This instrument provides the non- destructive method for the measurement of LAI. It determines LAI by measuring the transmission of radiation through the canopy above and below the canopy layers (gap fraction method) (Breda 2003). The LAI measurements were taken during sufficient sunlight required for accurate measurement (i.e. calibration point of view). The LAI measurements were taken at five different locations in all the sampling fields during in-situ measurements. For each location, a single above canopy reading followed by three below-canopies readings were taken for the LAI measurement. The measurements above the canopy serve as a reference. The average of five LAI measurements was taken to compute the average value of the LAI.

Figure 2.2 Leaf Area Index (LAI)-2200C Plant Canopy Analyzer

2.2.2 Soil moisture (M_v) measurement

The soil moisture (M_v) of the soil is defined as the ratio of the weight of water present in the soil to the weight of dry soil. It can also be expressed as a percentage of M_v. Five random soil samples were collected in the soil field up to a depth of 15 cm from the soil surface. This strategy was applied for all visited sampling fields under study. All these soil samples were dried in an oven at 100-110 ^{0}C for 24 hours. The soil samples were weighed before and after drying to compute the M_v. The average of the five soil samples were taken to calculate the percentage of M_v of the soil surface for entire sampling points. The procedure and requirement to compute the M_v are described as below,

2.2.2.1 Requirements

i. Oven with 100 -110 °C temperature range for drying the soil samples.

ii. A balance of precision of ± 0.001 g for weighing the soil samples.

iii. The metallic soil container and tube Auger for taking soil samples from the ground surface.

2.2.2.2 Procedure to determine the soil moisture (M_v)

i. Taking the soil samples in the soil container from the ground surface up to the depth of 15 cm about a 50 to 200 g. The weight of the wet soil samples was measured.

ii. The soil sample was placed in the oven at 100 °C for 24 hours or overnight after weighing the wet soil sample.

iii. After the drying of the soil sample, the weight of the dry soil sample was measured.

2.2.2.3 Soil moisture (M_v) computation

The M_v on a dry weight basis were computed using Equation (2.5) (Singh 2005).

$$M_v = \frac{(weight\ of\ wet\ soil\ sample) - (weight\ of\ dry\ soil\ sample)}{(weight\ of dry\ soil\ sample)} \qquad (2.5)$$

2.2.3 Surface roughness measurement

For the surface roughness parameters, a one-meter long metallic plate painted with the grid of an area of 1 cm^2 was used for the measurement of soil surface roughness, as shown in Figure 2.3. The metallic plate was pushed into the surface until the grid line reached at the lowest point on the soil surface. The surface roughness profile was drawn on the metallic plate using an ink marker, as shown in Figure 2.4. After that the photograph of the surface roughness profile was taken and then later digitized from the photograph. The advantage of this approach is that the equipment is relatively cheap and easily operated in the field for the measurement of soil surface roughness (Oh et al. 1992; Elachi, and Van Zyl 2006).

2.2.3.1 Root mean square (RMS) height (s) measurement

The surface height variation $z(x)$ of a random surface can be considered as the function of horizontal distance (x) across the mean surface. The surface height variations across its horizontal distance can be extracted from the photograph of a rough surface profile.

The surface roughness profile is digitized into discrete values $z_i(x_i)$ at an appropriate spacing Δx. This data contains the vertical surface heights (cm) at the horizontal spacing of 1 cm above and below the mean surface height. In the present investigation, 100 data points were acquired from the digitized photograph.

The root mean square height (s) of the discrete one-dimensional surface roughness profile is given as

$$s = \left[\frac{1}{N-1}\left(\sum_{1}^{N} z_i^2 - N\bar{z}^2\right)\right]^{\frac{1}{2}} \tag{2.6}$$

Where N is the number of samples and

$$\bar{z} = \frac{1}{N}\sum_{i=1}^{N} z_i \tag{2.7}$$

Where $\bar{z}$ is the mean surface of the surface height variation.

2.2.3.2 Auto correlation function and correlation length (l) measurement

The statistical variation of a random surface is characterized by its root mean square height (s) and its autocorrelation function $\rho(\xi)$. The detailed procedure for the measurement of surface height variation $z(x)$ of typical one-dimensional random rough surface profile as a function of horizontal distance (x) is presented in the above subsection.

The surface autocorrelation function is a measure of the degree of correlation between the surface height variation $z(x)$ at a point x on horizontal scale of the surface profile and the surface height variation $z(x + \xi)$ at a point ξ distance from x. The autocorrelation function of the discrete one-dimensional surface can be expressed by Equation (2.8) as

$$\rho(\xi) = \frac{\sum_{i=1}^{N+1-j} z_i z_{j+i-1}}{\sum_{i=1}^{N} z_i^2} \tag{2.8}$$

Where $\xi = (j-1)\,\Delta x$ and j is an integer ≥ 1.

The correlation length (l) of a rough surface is defined as the displacement ξ for which $\rho(\xi)$ is equal to e^{-1}

$$\rho(l) = e^{-1} \tag{2.9}$$

The value of l is small for a surface with a rapidly varying height profile, whereas for a perfectly smooth surface in which every point is perfectly correlated with every other point, l is infinite. In general, the RMS height (s) is a measure of the vertical roughness of the surface, and correlation length (l) is a measure of the horizontal roughness.

Theoretical surface scattering models have been formulated in terms of the autocorrelation function of the surface $\rho(\xi)$. Several mathematical forms have been used in the literature to describe autocorrelation function $\rho(\xi)$ of the natural surfaces (Oh et al. 1992). For example, these includes

$$Gaussian: \qquad \rho_1(\xi) = \exp\left(-\frac{\xi^2}{l^2}\right) \tag{2.10}$$

$$Exponential: \qquad \rho_2(\xi) = \exp\left(-\sqrt{2}\frac{\xi}{l}\right) \tag{2.11}$$

These theoretical autocorrelation functions do not provide good agreement to measure autocorrelation functions of real surface, particularly for displacements exceeding $\xi = l$. This is the limitation of representing the statistical height variations of real surfaces, which are responsible for the relatively poor agreement between the theoretically and experimentally observed radar responses to the surface roughness.

Figure 2.3 Metallic plate (1 meter long) used for the measurement of soil surface roughness

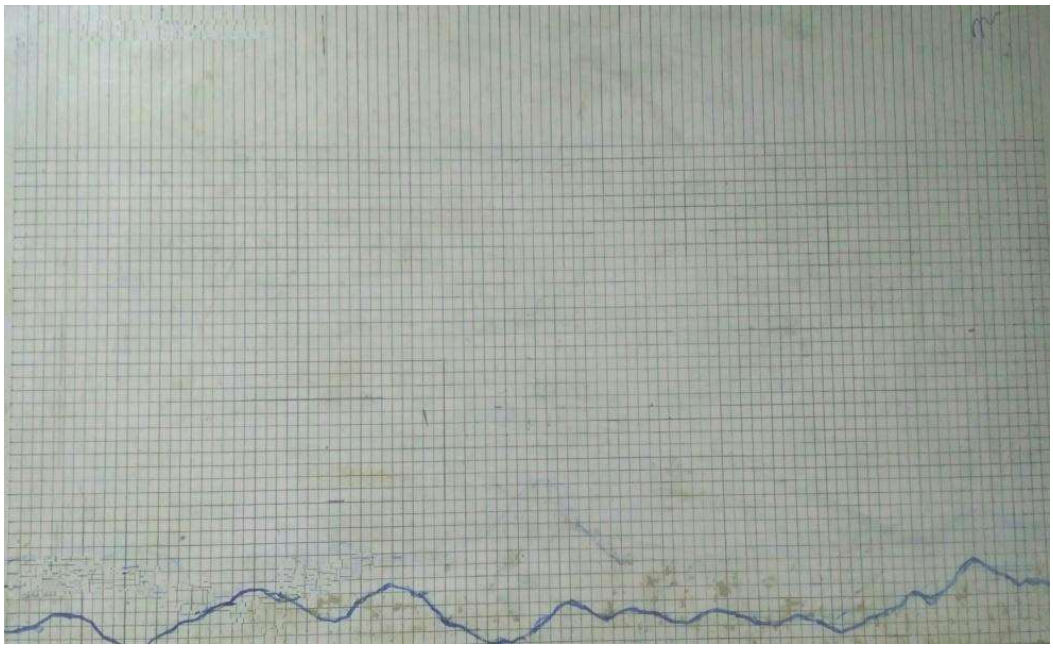

Figure 2.4 The surface roughness profile drawn on the metallic plate using ink marker

2.3 METHODOLOGY

Figure 2.5 shows the general work flow for present thesis work starting from collecting the satellite images developing intermediate modelling and computational techniques steps for the retrieval of biophysical and soil moisture. The inversion algorithm (LUT and MTRFR), statistical performance indices and advance machine-learning computational algorithms were incorporated for the parameterization (non -linear least square and genetic optimization model) and retrieval of indirect parameters (LAI, LWAI and M_v) of scattering algorithms.

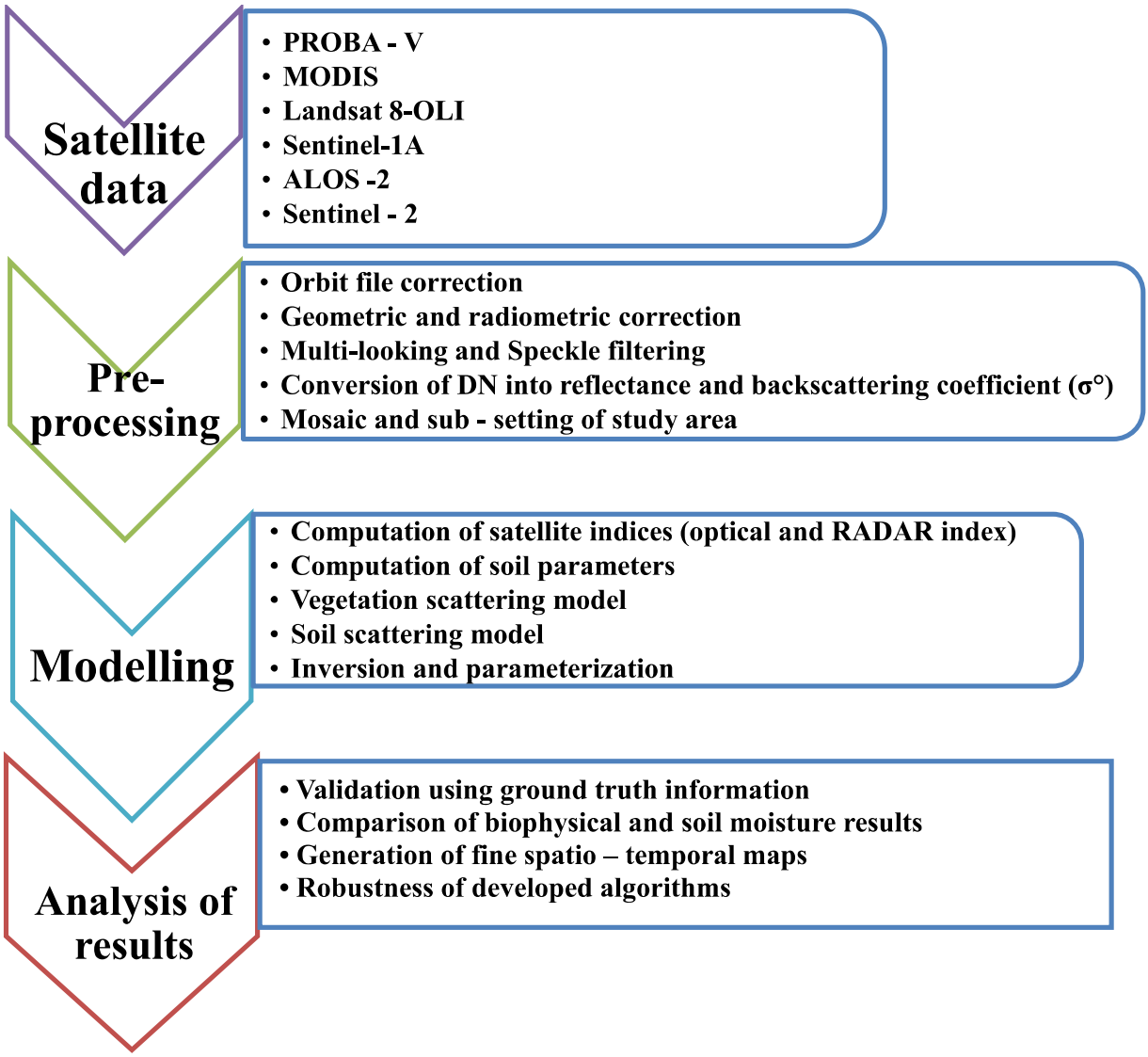

Figure 2.5 The schematic flowchart of the methodology for present research work

2.3.1 Microwave backscattering modelling

Figure 2.6 shows the schematic diagram of the SAR backscattering mechanism over the vegetation and soil interfaces. The total backscatter coefficient (σ_T^0) depends on the various system (sensor properties) and Earth target parameters (Ulaby et al. 1990). The frequency, incidence angle (θ), and polarizations (HH, VV, HV and VH) are the sensor parameters onboard satellite and dielectric constant (ε_s), temperature, orientation, and surface roughness (M_v, s, l) are the Earth target parameters. The onboard satellite sensor parameters are the core of SAR image processing which significantly influences the electromagnetic signals that are backscattered toward the sensor (Karam et al. 1995). However, the required parameter is extracted by minimizing the influence of others using various modelling techniques (Jones et al. 2011). The on–board satellite sensor parameters are static and controllable whereas the target parameters are highly dynamic which are responsible for quantifying the information about the Earth surface targets.

Generally, the σ_T^0 from vegetated pixels mainly expressed as the sum of contributions due to (i) volume scattering $\sigma_{veg}^0(V)$ from the vegetation canopy itself, (ii) surface scattering $\sigma_{soil}^0(\varepsilon_s, M_v, \theta)$ by the soil attenuated by the vegetation layer, and (iii) intermediate interactions $\sigma_{inter}^0(\varepsilon_s, M_v, \theta, V)$ between the canopy and the ground surface composed of volume scattering generated from the direct backscattering of the vegetation and the soil surface after the double attenuation, as follows :

$$\sigma_T^0 = \sigma_{veg}^0(V) + \sigma_{inter}^0(\varepsilon_s, M_v, \theta, V) + \tau^2 \sigma_{soil}^0(\varepsilon_s, M_v, \theta) \qquad (2.12)$$

where σ_{veg}^0 represents the backscattered radar signal from vegetation canopy and σ_{soil}^0 is the backscattering response from bare soil surfaces. Whereas, the $\tau^2 = \exp\left(\frac{-2 \times B \times V}{cos\theta}\right)$ is defined as two-way attenuation factor through vegetation-soil interfaces.

The $\sigma^0_{veg}(V)$ records the backscattered signal from the vegetation canopy (i.e. volume scattering) or from homogeneous vegetation surface (coherent scattering). Equation (2.13) expressed the numerical modelling of vegetation backscattered signal which directly and indirectly depend on the sensor parameter and vegetation surface parameters. The model parameters like A, E and B were included the both system and surface parameters.

$$\sigma^0_{\text{veg}} = AV^E cos\theta \left[1 - \exp\left(\frac{-2 \times B \times V}{cos\theta}\right)\right] \quad (2.13)$$

Moreover, the σ^0_{soil} is defined as backscattered echoes from the soil surface (vegetated soil and bare soil surfaces). In the present thesis, a comprehensive theoretical analysis of the various modified geometrical soil scattering and advance physical soil scattering algorithms (Oh model, IEM model and empirical algorithm) were incorporated for completeness of soil surface conditions.

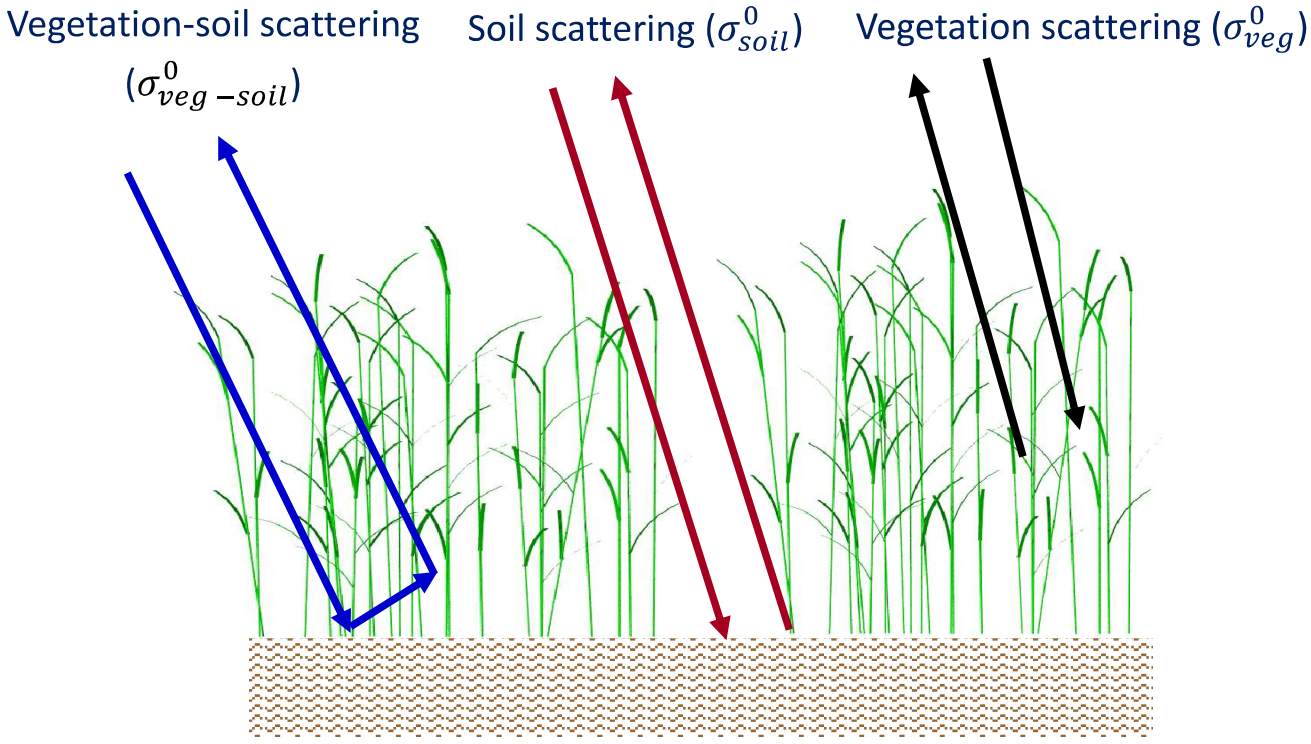

Figure 2.6 The SAR backscattering phenomenon over the vegetation and soil layers

2.3.2 Computation of dual polarimetric radar vegetation index

The other part of the present thesis is to study the polarimetric index behavior of SAR signal for crop growth monitoring. The dual polarimetric Sentinel -1A (VV + VH) and ALOS – 2 (HH + HV) SAR satellite were used for the computation of polarimetric radar vegetation index. These indexes can be more useful for the study of spatial and temporal variations in crop growth and changes in their phenology stages. In this study, the scattering information in terms of the degree of polarization (m) and the eigenvalue spectrum (λ_1 and λ_2) were jointly utilized to compute the radar vegetation index at C- and L- bands microwave frequencies. Subsequently, the calculation of dual polarimetric radar index values are discussed step by steps as below:

2.3.2.1 Computation of Radar Vegetation Index from ALOS -2 (L- band) SAR satellite data

The full details description about of polarimetric radar vegetation index computation using ALOS-2 at HH and HV polarizations are shown in Figure 2.7. The polarimetric 2 × 2 covariance scattering matrix (C_2^L) were derived using average real and imaginary scattering vectors for L - band, which is given below:

$$C_2^L = \begin{bmatrix} C_{11} & C_{12} \\ C_{21} & C_{22} \end{bmatrix} = \begin{bmatrix} < |s_{HH}|^2 > & < s_{HH}\, s_{HV}^* > \\ < s_{HV}\, s_{HH}^* > & < |s_{HV}|^2 > \end{bmatrix} \qquad (2.14)$$

Equation (2.15) represents the degree of polarization (m_L) used to express the polarization state of electromagnetic (EM) wave. The value m_L = 1 is for complete polarization of EM wave and m_L = 0 is for completely unpolarized EM wave. For the partially polarized, it varies in between $0 < m_L < 1$. The decomposition of polarimetric (unitary transformation) techniques were adopted for computation of eigenvalues of above 2 × 2 covariance scattering matrix. Whereas, the $|C_2^L| = \lambda_1 \lambda_2$ is defined as the determinant of matrix and Tr (C_2^L) =

$\lambda_1 + \lambda_2$ represents the trace (i.e. sum of eigenvalues) of matrix. These λ_1 and λ_2 characterizes the dominancy in the scattering mechanism. If $\lambda_1 \geq \lambda_2$, the single scattering mechanism is dominant (i.e. direct scattering from the homogeneous vegetation canopy).

$$m_L = \sqrt{1 - \frac{4\left|C_2^L\right|}{(\mathrm{Tr}\,(C_2^L))^2}} \qquad (2.15)$$

Therefore, with help of above computational techniques and scattering matrix parameters, the radar vegetation index was calculated (viz. D_pRVI , PRVI and RVI) using ALOS - 2 (L - band) data. The mathematical expression for polarimetric radar vegetation index discussed is shown as follows:

(I) Dual polarimetric radar vegetation index (D_pRVI) at L – band (1.2 GHz)

$$D_pRVI = 1 - m_L\beta \qquad 0 \leq D_pRVI \geq 1 \qquad (2.16)$$

$$\beta = \frac{\lambda_1}{\lambda_1 + \lambda_2}$$

(II) Polarimetric radar vegetation index (PRVI) at L- band (1.2 GHz)

$$PRVI = (1 - m_L)\,\sigma^0_{HV} \qquad (2.17)$$

(III) Radar vegetation index (RVI) at L- band (1.2 GHz)

$$RVI = \frac{4\,\sigma^0_{HV}}{\sigma^0_{HH} + \sigma^0_{HV}} \qquad (2.18)$$

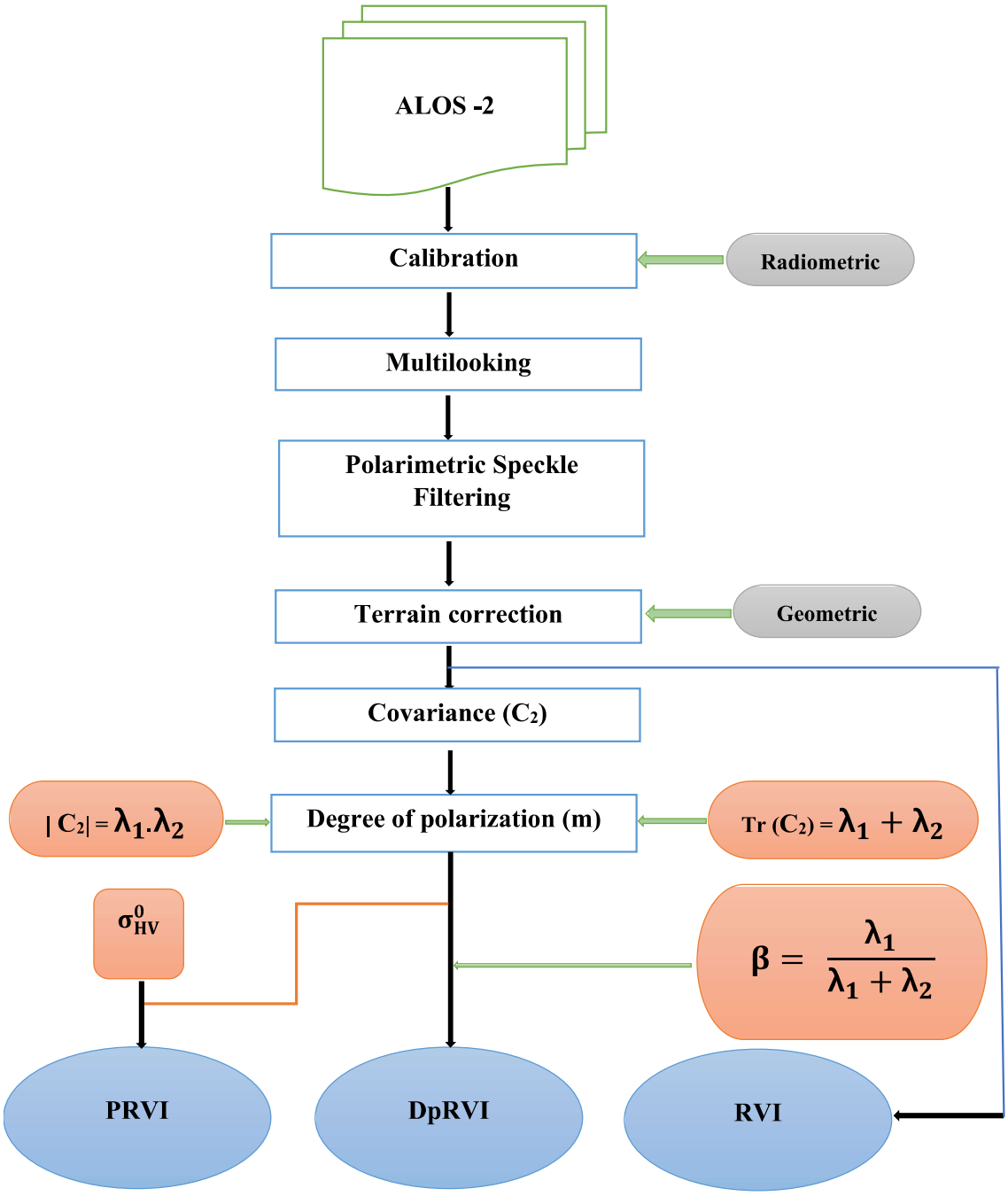

Figure 2.7 Flowchart for the computation of dual polarimetric radar vegetation index using ALOS - 2 SAR satellite data at HH and HV polarization

2.3.2.2 Computation of Radar Vegetation Index from Sentinel-1A (C - band) SAR data

The study of polarimetric responses using Sentinel-1A SAR data is quite complex than ALOS-2 SAR data. Figure 2.8 shows the complete step by step pre-processing method and computation of polarimetric radar vegetation index from Sentinel - 1A (SLC) images. The C_2^C and m_C are the 2 × 2 covariance scattering matrix and degree of polarization at VV + VH polarization, respectively.

$$C_2^C = \begin{bmatrix} C_{11} & C_{12} \\ C_{21} & C_{22} \end{bmatrix} = \begin{bmatrix} < |S_{VV}|^2 > & < S_{VV}\, S_{VH}^* > \\ < S_{VH}\, S_{VV}^* > & < |S_{VH}|^2 > \end{bmatrix} \quad (2.19)$$

$$m_C = \sqrt{1 - \frac{4|C_2^C|}{(\mathrm{Tr}\,(C_2^C))^2}} \quad (2.20)$$

The mathematical expression for various polarimetric radar vegetation indexes using Sentinel - 1A (C - band) at VV and VH polarization is given below:

(I) Dual polarimetric radar vegetation index (D_pRVI) at C- band (5.405 GHz)

$$D_p\mathrm{RVI} = 1 - m_C\beta \qquad 0 \leq D_p\mathrm{RVI} \geq 1 \quad (2.21)$$

$$\beta = \frac{\lambda_1}{\lambda_1 + \lambda_2}$$

(II) Polarimetric radar vegetation index (PRVI) at C- band (5.405 GHz)

$$P\mathrm{RVI} = (1 - m_C)\,\sigma_{VH}^0 \quad (2.22)$$

(III) Radar vegetation index (RVI) at C- band (5.405 GHz)

$$\mathrm{RVI} = \frac{4\,\sigma_{VH}^0}{\sigma_{VV}^0 + \sigma_{VH}^0} \quad (2.23)$$

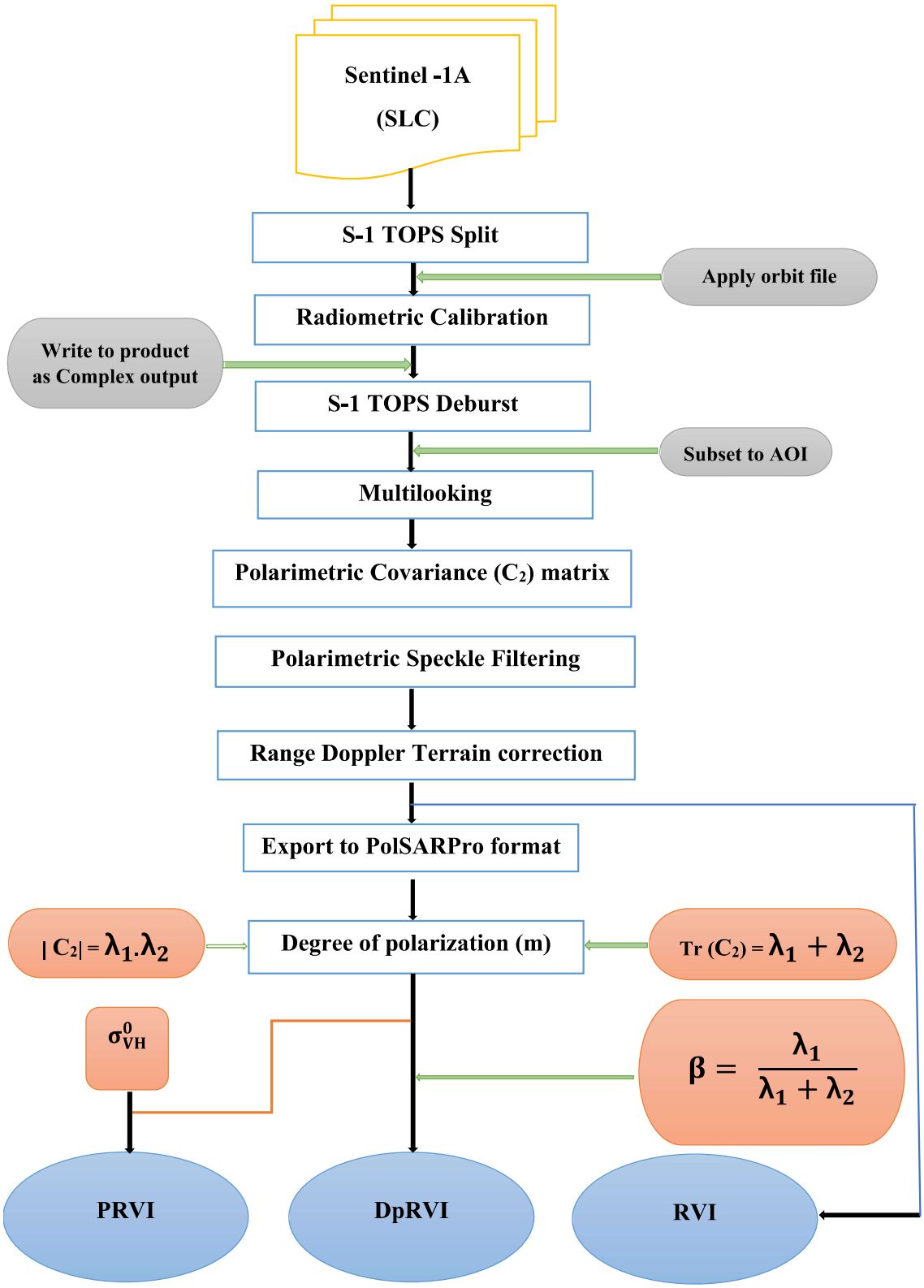

Figure 2.8 Flowchart for the computation of dual polarimetric radar vegetation index using Sentinel -1A SAR satellite data at VV and VH polarizations

2.3.3 Calculation of optical spectral indices

The computations of different optical spectral indices used in the present thesis are shown in the Table 2.4. The indices are the mathematical equation which contains the spectral reflectance values from various regions of electromagnetic spectrum. These indices classify and discriminate the Earth surface features using the reflectance values of a particular wavelength range. For the computation of the vegetation index used in the study, the reflectance values from mainly NIR and Red band are used. The healthy vegetation shows very high reflectance values in the NIR band and very low reflectance values in case of Red band due to availability of more chlorophyll content (Figure 2.9). This indicates the green vegetation present in an image using NDVI. The Red - Edge (RE) determines the rapid change of vegetation reflectance value in RED to NIR transition regions, which is shown in Figure 2.10. The RE indices are more sensitive for vegetation to classify the crop patterns, growth conditions and stress condition. However, the f_{veg} values were derived for the weightage of correct amount of vegetation, soil and intermediate effect within a pixel.

Table 2.4 Equations used for the calculation of spectral indices

Spectral Indices	**Equations**
Normalized Difference Vegetation Index (NDVI)	$\frac{NIR - RED}{NIR + RED}$
Red-Edge normalized difference vegetation index ($NDVI_{RE}$)	$\frac{(NIR - RE)}{(NIR + RE)}$
Modified simple ratio Red-Edge (MSR_{RE})	$\frac{(NIR/RE - 1)}{(\sqrt{NIR/RE + 1})}$
Chlorophyll index Red-Edge (CI_{RE})	$\frac{NIR}{RE} - 1$
Vegetation fraction (f_{veg})	$\frac{NDVI - NDVI_{min}}{NDVI_{max} - NDVI_{min}}$

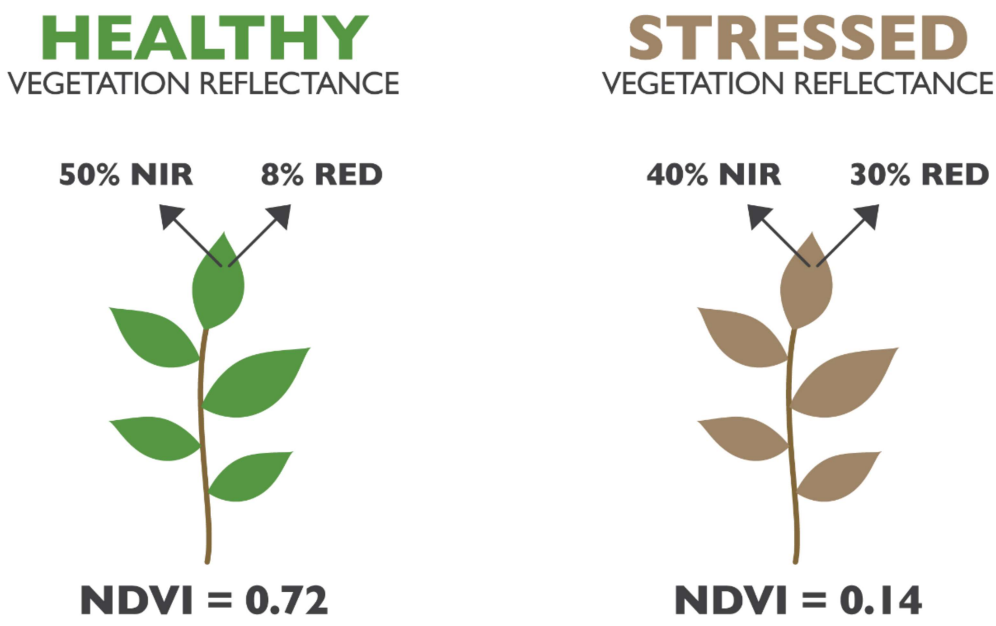

Figure 2.9 NDVI value for healthy and stress vegetation

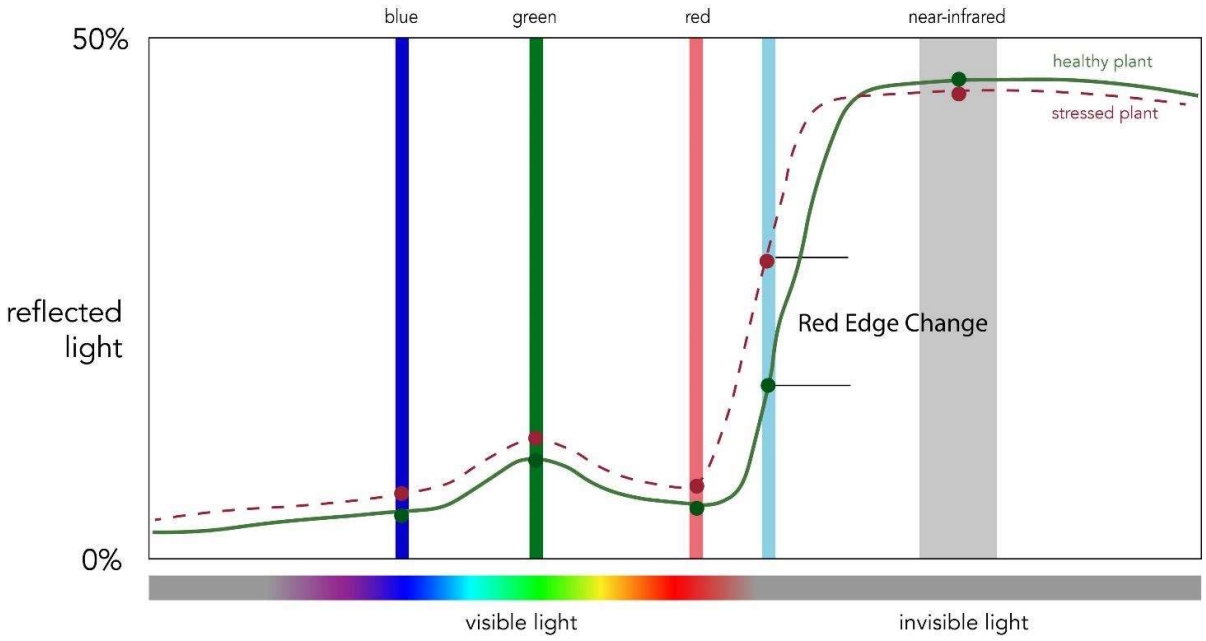

Figure 2.10 Spectral reflectance curve for healthy and stress plant and Red - Edge (RE) region

(**Source**: https://miro.medium.com/max/8102/1*bImZ5n-V8LkjSFyjVexpBQ.jpeg)